Boundary-Layer Meteorol (2009) 130:275–300
DOI 10.1007/s10546-008-9348-0

ORIGINAL PAPER

Attenuation of Scalar Fluxes Measured with Spatially-displaced Sensors

T. W. Horst · D. H. Lenschow

Received: 5 May 2008 / Accepted: 22 December 2008 / Published online: 9 January 2009
© Springer Science+Business Media B.V. 2009

Abstract Observations from the Horizontal Array Turbulence Study (HATS) field program are used to examine the attenuation of measured scalar fluxes caused by spatial separation between the vertical velocity and scalar sensors. The HATS data show that flux attenuation for streamwise, crosswind, and vertical sensor displacements are each a function of a dimensionless, stability-dependent parameter n_m multiplied by the ratio of sensor displacement to measurement height. The scalar flux decays more rapidly with crosswind displacements than for streamwise displacements and decays more rapidly for stable stratification than for unstable stratification. The cospectral flux attenuation model of Kristensen et al. agrees well with the HATS data for streamwise sensor displacements, although it is necessary to include a neglected quadrature spectrum term to explain the observation that flux attenuation is often less with the scalar sensor downwind of the anemometer than for the opposite configuration. A simpler exponential decay model provides good estimates for crosswind sensor displacements, as well as for streamwise sensor displacements with stable stratification. A model similar to that of Lee and Black correctly predicts flux attenuation for a combination of streamwise and crosswind displacements, i.e. as a function of wind direction relative to the sensor displacement. The HATS data for vertical sensor displacements extend the near-neutral results of Kristensen et al. to diabatic stratification and confirm their finding that flux attenuation is less with the scalar sensor located below the anemometer than if the scalar sensor is displaced an equal distance either horizontally or above the anemometer.

Keywords Flux attenuation · Flux sensor separation · Scalar flux measurement · Spatial turbulence structure · Taylor's hypothesis

1 Introduction

Turbulent fluxes of scalar atmospheric constituents are determined by correlating a time series of vertical velocity measurements, commonly made using a tower-mounted sonic

T. W. Horst (✉) · D. H. Lenschow
National Center for Atmospheric Research, Boulder, CO, USA
e-mail: horst@ucar.edu

anemometer, with a time series of scalar density measurements made by an appropriate fast response sensor, e.g. an open-path optical-absorption hygrometer in the case of water vapour fluxes. In order to avoid flow distortion errors in the velocity measurements, in-situ scalar sensors must be displaced from the measurement volume of the sonic anemometer (Wyngaard 1988). Unfortunately this causes a decorrelation of the velocity and scalar density measurements and a reduction in the measured flux. Kristensen et al. (1997) observed that the attenuation of the measured flux "must be an increasing function of the ratio of the sensor displacement and the scale of the turbulence". In the atmospheric surface layer, the integral scale of the vertical velocity component increases with height (e.g. Kaimal and Finnigan 1994), and therefore the flux attenuation will increase with the ratio of sensor displacement to the measurement height. Once the flux attenuation is known, the measured flux can be corrected simply by dividing it by the estimated fractional attenuation.

Two recent articles have examined this issue with extensive datasets that use temperature as the measured scalar variable, with the assumption that by scalar similarity the observed attenuation in the heat flux can be applied equally as well to other scalar fluxes (Hill 1989). Lee and Black (1994, hereafter LB) collected data during neutral to unstable stratification using two horizontal, linear, orthogonal arrays of five thermocouples each, combined with a vertical-axis sonic anemometer and thermocouple co-located at the intersection of the two thermocouple arrays. They computed the displaced scalar flux $F(r_x, r_y)$ by eddy covariance using thermocouples displaced from the sonic anemometer by r/z ranging from 0.07 to 1.23, and they also computed the scalar flux with co-located sensors, $F_o \equiv F(0, 0)$. Here (r_x, r_y) are the streamwise and crosswind sensor displacements, $r^2 \equiv r_x^2 + r_y^2$, and z is the measurement height.

LB found that their observed fluxes were in good agreement with their theoretical/empirical relation

$$F(r_x, r_y) = F_o \exp[-\alpha(\theta)\phi_h\phi_\epsilon^{1/3}(r/z)^{4/3}], \tag{1}$$

where $\phi_h(z/L)$ and $\phi_\epsilon(z/L)$ are the usual dimensionless stability functions that describe the dependence of the vertical potential temperature gradient and turbulent dissipation on atmospheric stability, z/L, where L is the Obukhov length. LB derived the functional dependence of $F(r_x, r_y)$ on z/L and $(r/z)^{4/3}$ with the assumption of inertial-range scaling, that is, the sensor displacement was assumed to be small enough to be comparable to inertial-range turbulence scales.

The dependence of Eq. 1 on wind direction is given as

$$\alpha(\theta) = 1.18(\cos^2\theta + 2.4\sin^2\theta)^{2/3}, \tag{2}$$

where θ is the wind direction with respect to the direction of the scalar sensor displacement (Fig. 1). LB derived the wind direction dependence with the assumption that the turbulent eddies have an elliptical shape in the horizontal, while the numerical coefficients in (2) were found from an empirical fit to their observations. Equation 2 implies that the decorrelation of vertical velocity and temperature is noticeably more sensitive to crosswind displacement ($\theta = \pi/2$) than to streamwise displacement ($\theta = 0$).

Kristensen et al. (1997, hereafter KMOW) measured scalar flux attenuation caused by both horizontal and vertical displacements. The fluxes with horizontal displacements were measured for three values of r/z, 0.083, 0.17 and 0.25, and 90% of their data fall within the ranges $-2 < z/L < 0$ and $|90° - \theta| < 45°$ (equivalently, $r_y > r_x$). Within these ranges, KMOW did not observe "any systematic variation" of $F(r_x, r_y)/F_o$ with wind direction and "no large

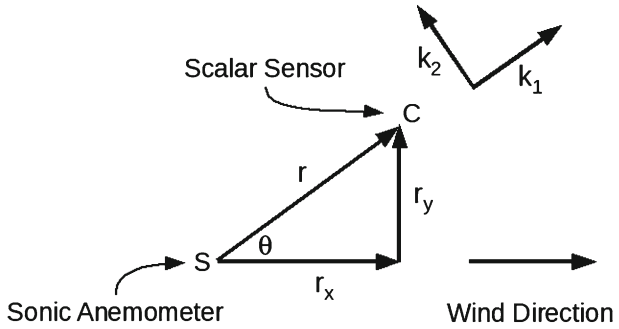

Fig. 1 Schematic of coordinate systems for displacement and wavenumber

variation" with stability. Then, with the assumption that $F(r_x, r_y)/F_o$ is independent of wind direction, they find

$$F(r_x, r_y) = \int_{-\infty}^{\infty} Co_{wc}(k) \cos(k\, r)\, \mathrm{d}k, \tag{3}$$

where k is wavenumber and $Co_{wc}(k)$ is the cospectrum for co-located measurements of vertical velocity and scalar density. KMOW model the cospectrum by fitting observations to

$$Co(k) = \frac{A(\mu) F_o}{k_m [1 + 0.75(k/k_m)^{2\mu}]^{7/6\mu}}, \tag{4}$$

where $k_m = 2\pi n_m / z$ is the wavenumber at the peak of the wavenumber-weighted co-spectrum $kCo(k)$, $n_m = f_m z/U$, f_m is the frequency at the peak of the cospectrum, and U is wind speed. Using $\mu = 0.23$ and $n_m = 0.07$, KMOW find that the predictions of Eqs. 3, 4 provide a reasonable match to their data. Since their data and the predictions of Eqs. 3, 4 both fall within the range predicted by Eqs. 1, 2 for the meteorological conditions of their experiment, $\theta \simeq 60°$ and $-2 < z/L < 0$, KMOW also note that "our measurement and theory are not in direct contradiction with Lee and Black".

KMOW also examined scalar flux attenuation for vertical sensor displacements, plotting the results as $F(z, z')/F_o$ versus z/z' where z is the height of the anemometer and z' is the height of the scalar sensor. They find the unexpected result that the flux attenuation is considerably less when the scalar sensor is below the anemometer, $z/z' > 1$, than if the scalar sensor is displaced an equal distance either horizontally or above the anemometer. Their data cover the range $0.4 < z/z' < 2.5$ and are fit reasonably well by

$$F(z, z')/F_o \equiv g(z/z') = \begin{cases} 1 - 1.0[1 - (z/z')], & z < z', \\ 1 - 0.1[(z/z') - 1], & z > z'. \end{cases} \tag{5}$$

KMOW explain heuristically how the asymmetry is caused by the dependence of the vertical scalar gradient on height, but their theoretical development does not lend itself to a quantitative prediction of flux attenuation and hence they are limited to the empirical Eq. 5.

Despite the valuable field observations and the theoretical advances found in Lee and Black (1994) and Kristensen et al. (1997), there remain contradictions between these two studies and the ranges of both sets of data are limited. LB observe a dependence of $F(r_x, r_y)/F_o$ on $(r/z)^{4/3}$, which theoretically should only apply for very small sensor displacements, and also find a dependence on stability and wind direction that apparently is not observed in the KMOW data. Further, neither of the two studies contains a significant quantity of data for

horizontal displacements in stable stratification. Finally, the KMOW vertical sensor displacement data apparently also exhibit minimal dependence on stability, despite including data with negative heat fluxes. This seems at variance with the stated expectation that the measured flux attenuation should be an increasing function of the ratio of sensor displacement and the scale of the turbulence.

The present study sheds some light on these questions using a recent dataset from the Horizontal Array Turbulence Study (HATS) field project. Section 2 contains a theoretical analysis of the issues and a suggestion for yet another relation for flux attenuation caused by spatial sensor separation. Section 3 describes the HATS dataset, which is then applied in Sect. 4 to the examination of horizontal displacements and in Sect. 5 to vertical displacements. Section 4 first treats streamwise and crosswind displacements separately and then suggests an analytical relation to combine those two results for any wind direction with respect to the sensor displacement. Finally, we note that our study does not address momentum fluxes, since current sonic anemometers commonly do not measure the three individual components of velocity at significantly separated locations (e.g. Horst and Oncley 2006).

2 Theoretical Analysis

The cross-covariance of turbulent fluctuations measured with a horizontal displacement $\mathbf{r}$ between the scalar sensor and the anemometer is

$$\begin{aligned}\overline{w'(\mathbf{x})\,c'(\mathbf{x}+\mathbf{r})} &= \int\int\int_{-\infty}^{\infty} e^{-i\mathbf{k}\cdot\mathbf{r}}\Phi_{wc}(\mathbf{k})\,\mathrm{d}^3k \\ &= \int_{-\infty}^{\infty} e^{-ik_1 r}\,Cr_{wc}(k_1)\,\mathrm{d}k_1 \end{aligned} \tag{6}$$

(e.g. Lumley and Panofsky 1964, p. 26ff). Here $\Phi_{wc}(\mathbf{k})$ is the three-dimensional cross spectrum between vertical velocity and scalar density fluctuations at the same location, k_1 is the wavenumber parallel to the spatial displacement, i.e. $\mathbf{k}\cdot\mathbf{r} = k_x r_x + k_y r_y \equiv k_1 r$ (Fig. 1), and $Cr_{wc}(k_1)$ is the one-dimensional cross spectrum along k_1,

$$Cr_{wc}(k_1) \equiv \int\int_{-\infty}^{\infty} \Phi_{wc}(\mathbf{k})\,\mathrm{d}k_2\mathrm{d}k_3. \tag{7}$$

Here k_2 and k_3 are horizontal and vertical coordinates normal to k_1. The cross spectrum can be separated into real and imaginary parts,

$$Cr_{wc}(k_1) = Co_{wc}(k_1) - i\,Q_{wc}(k_1), \tag{8}$$

where $Co_{wc}(k_1)$ and $Q_{wc}(k_1)$ are the one-dimensional cospectrum and quadrature spectrum respectively. After substituting Eq. 8 into 6 and expanding the exponential, we note that the imaginary terms integrate to zero because $Co_{wc}(k_1)\sin(k_1 r)$ and $Q_{wc}(k_1)\cos(k_1 r)$ are antisymmetric functions of k_1. Thus we find

$$F(\mathbf{r}) = \int_{-\infty}^{\infty} \left[Co_{wc}(k_1)\cos(k_1 r) - Q_{wc}(k_1)\sin(k_1 r)\right]\,\mathrm{d}k_1. \tag{9}$$

Note that the first term in Eq. 9 is a symmetric function of sensor displacement r, and the second term is an antisymmetric function of r. We expect the integral of the second term to be zero for crosswind sensor displacements because there is no obvious physical reason for $F(r_y)$ to be antisymmetric. However, it will be seen in Sect. 4.1 that for streamwise displacements, $F(r_x)$ is observed to differ for upwind and downwind displacements, implying

a contribution of the quadrature spectrum to fluxes measured with sensors displaced in the streamwise direction. Finally, we caution that the foregoing analysis applies only for spatially homogeneous turbulence and thus does not apply to vertical sensor displacements in the atmospheric surface layer.

If it is assumed as in KMOW that $\Phi_{wc}(\mathbf{k})$ is axisymmetric with respect to the vertical coordinate, then the quadrature spectrum is identically zero and Eq. 3 follows from Eq. 9. In the more general case, Eq. 9 is most useful when $\mathbf{r}$ is in the streamwise direction, because with the assumption of Taylor's hypothesis we can estimate $Co\,(k_x)$ and $Q\,(k_x)$ from time series data. Equation 9 is less useful for crosswind displacements because we commonly do not know the dependence of the cospectra on the crosswind wavenumber.

Additional insight can be obtained by assuming that the KMOW one-dimensional cospectrum, Eq. 4, applies in all directions and that the quadrature spectrum is negligible. Then Eq. 9 can be written as

$$F(\mathbf{r}) = A(\mu)F_o \int_{-\infty}^{\infty} \frac{\cos(k_{1m}r\kappa)}{[1 + 0.75\kappa^{2\mu}]^{7/6\mu}}\,\mathrm{d}\kappa, \tag{10}$$

where $\kappa = k_1/k_{1m}$ and k_{1m} is the wavenumber at the maximum of the wavenumber-multiplied cospectrum for the wavenumber parallel to $\mathbf{r}$. Thus we obtain the useful result that $F(\mathbf{r}) = f(k_{1m}r, \mu)$. The independent variable $k_{1m}r$ can be written either in the form $2\pi r/\lambda_{1m}$, where λ_{1m} is the wavelength of the cospectral maximum parallel to the sensor displacement, or in the form $2\pi n_{1m}r/z$, where $n_{1m} = z/\lambda_{1m}$ is a dimensionless function of stability (Kaimal et al. 1972). Thus the independent variable $k_{1m}r$ contains explicitly the expected dependence on r/λ_{1m} or r/z noted in the Introduction, as well as an implicit dependence on stability and wind direction. Using the HATS data, to be described in the next section, we find that the KMOW cospectrum provides a reasonable fit to streamwise cospectra with $\mu \simeq 1/4$ for unstable stratification and $\mu \simeq 1/2$ for stable stratification (Appendix A). Using the KMOW cospectrum, we can then estimate flux attenuation by numerically integrating (10) and investigating its dependence on $k_{1m}r$ and stability.

We first examine the result of LB that the flux attenuation depends on $(r/z)^{4/3}$. Assuming a form of $Co\,(k)$ appropriate for locally isotropic turbulence, KMOW integrate Eq. 3 and obtain a result equivalent to that of LB for small r/z,

$$F(r) \approx F_o[1 - (9/4)B\,\Gamma(2/3)\,(r/z)^{4/3}], \tag{11}$$

where B is a stability-dependent parameter and Γ is the gamma function. Figure 2 shows the quantity $1 - F(r)/F_o$ as a function of $k_m r$, obtained by numerical integration of Eq. 3 or 10, using the KMOW/HATS stable and unstable cospectra and the Kansas neutral cospectrum of Kaimal et al. (1972). Also shown are asymptotes to these curves at small $k_m r$, corresponding to the locally isotropic result $1 - F(r)/F_o \sim (r/z)^{4/3}$. It can be seen that, for realistic cospectra, the flux attenuation is dependent on $(r/z)^{4/3}$ only for sensor displacements so small that $F(r)/F_o \geq 0.99$. (Fig. 2 shows that for a flux attenuation of 10%, Eq. 11 is clearly no longer valid for predicting $F(r)/F(r_o)$, but we note that Eq. 11 is still equivalent within 0.5% to Eq. 1.)

Alternately, an analytical relation for the flux attenuation can be obtained by assuming a cospectrum of the form,

$$Co(k) = \frac{2}{\pi k_m[1 + (k/k_m)^2]}. \tag{12}$$

Although this cospectrum departs from the theoretical inertial-range slope of $-7/3$ used in the KMOW cospectrum, Horst (1997) finds that it provides a close match to the Kansas stable

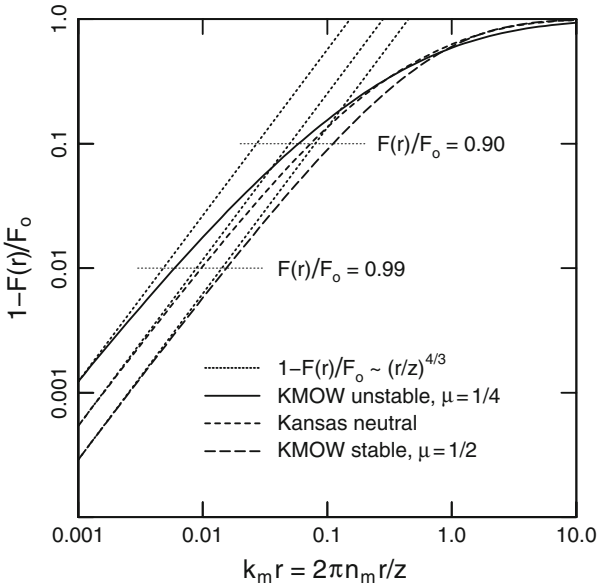

Fig. 2 Test of Eq. 1, $F(r)/F_o \sim (r/z)^{4/3}$

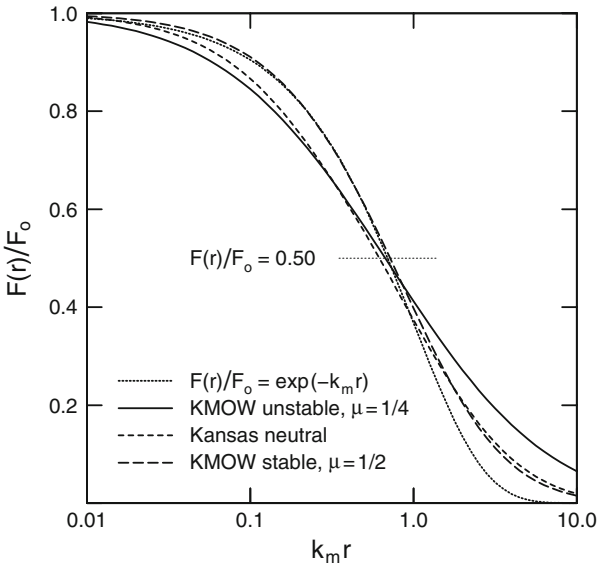

Fig. 3 Test of Eq. 13, $F(r)/F_o = \exp(-k_m r)$

cospectrum of Kaimal et al. (1972). With this cospectrum, Eq. 3 can be integrated analytically to obtain the simple relation

$$F(r) = F_o \exp(-k_m r). \tag{13}$$

Figure 3 shows $F(r)/F_o$ as a function of $k_m r$ for the same cospectra used in Fig. 2 and compares them to Eq. 13. The exponential formula departs significantly from the flux attenuation estimated for neutral and unstable stratification, but for stable stratification it provides a very good match for $0.5 \leq F(r)/F_o \leq 1$.

3 HATS Field Observations

The Horizontal Array Turbulence Study collected turbulence data from two parallel, horizontal arrays of sonic anemometers oriented in the climatological crosswind direction (Horst et al. 2004). The two parallel arrays, labeled s and d, were composed of five and nine equally-spaced sonic anemometers respectively, with one array located directly above the other as shown in Fig. 4. Table 1 lists the heights above the ground z_{agl} and sonic spacings S of the four HATS configurations. The range of $r/(z_{agl}-h_d)$ for the HATS sonic configurations is 0.13–8.56, where h_d is the zero-plane displacement. The following results were calculated from 49 stationary, 25–60 min periods that were selected to cover a wide range of stability from each of the four sonic configurations.

The HATS field measurements were obtained by the Integrated Surface Flux Facility (ISFF), which is maintained and operated by the Earth Observing Laboratory of the National Center for Atmospheric Research. Fourteen identical Campbell Scientific three-component sonic anemometer-thermometers (CSAT3) were used for the two horizontal lines of sonics and were programmed to provide data in the 'single-measurement' mode at a rate of 20 Hz. The prevailing wind direction was from the north-west, and thus the measurement site was located near the south-east corner of a 5-km square area of level, fallow farmland. The surface was covered with various mixtures of crop stubble and weeds, and the fields were crossed at roughly 60-m intervals by irrigation check dams that were oriented east to west and rose roughly 0.2–0.25 m above the level of the field. A zero-plane displacement of 0.32 m and a surface roughness length z_o of 20 mm were calculated from near-neutral wind profiles obtained at the site. A detailed description of the HATS field site and a discussion of sonic anemometer data processing and quality control analysis can be found at www.eol.ucar.edu.

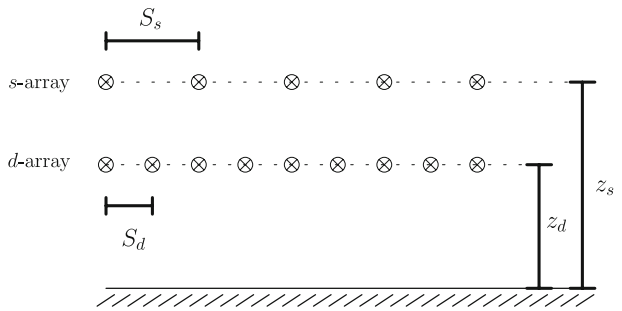

Fig. 4 Schematic of the two HATS horizontal sonic arrays at heights $\{z_d, z_s\}$ and with crosswind sonic separations $\{S_s, S_d\}$

Table 1 HATS transverse array dimensions (m). The zero-plane displacement h_d for the HATS site was found to be 0.32 m

Configuration	z_d (m agl)	S_d (m)	z_s (m agl)	S_s (m)
1	3.45	3.35	6.90	6.70
2	4.33	2.17	8.66	4.33
3	8.66	2.17	4.33	1.08
4	4.15	0.50	5.15	0.63

4 Horizontal Sensor Displacements

4.1 Streamwise Sensor Displacements

In order to investigate scalar flux attenuation caused by spatial sensor displacement, virtual temperature fluxes were calculated by correlating sonic anemometer measurements of vertical velocity w and temperature derived from the speed of sound T_c (Schotanus et al. 1983), that is $F_o = \overline{w' T_c'}$. The fluxes for streamwise sensor displacements were estimated from the HATS data by assuming Taylor's frozen-field approximation (Taylor 1938) and lagging the scalar (sonic temperature) time series by $\tau = r_x / U_a$ with respect to the vertical velocity time series for each sonic,

$$F(r_x) = \overline{w'(x,t)\, T_c'(x + U_a \tau, t)} = \overline{w'(x,t)\, T_c'(x, t-\tau)}. \tag{14}$$

Here U_a is an eddy advection velocity on the order of U, the mean wind speed at the measurement height, and which we will discuss further at the end of this section. Positive r_x corresponds to the scalar sensor downstream of the anemometer (Fig. 1). The flux attenuation was determined for each analysis period by dividing $F(r_x)$ by the co-located flux F_o for each sonic and then averaging the flux ratios over all sonics at a given height.

Figures 5a–c show the composited flux attenuation for unstable, weak stable, and strong stable stratification, as a function of $k_{mx}|r_x|$. Here k_{mx} were determined by fitting the KMOW cospectrum, Eq. 4, to the HATS streamwise cospectra (Appendix A) using $k_x = 2\pi f / U_a$, where f is frequency, again assuming Taylor's approximation. The observations are sorted into $k_{mx}|r_x|$ intervals and the data points are the medians of the measured flux attenuation within each bin. The vertical lines associated with each point denote the quantiles of its corresponding data distribution for 15 and 85% cumulative probability, which are equivalent to $\pm$ one standard deviation for a normal distribution.

Points are shown separately for positive and negative streamwise sensor displacements. Flux attenuation with the scalar sensor downwind of the sonic ($r_x > 0$) is systematically less than that for the opposite configuration, although the difference between the two displacements is often less than the total range of the data for each $k_{mx}|r_x|$ interval. The noticeable asymmetry for positive and negative displacements is present for all stabilities and is likely a consequence of the asymmetric ramp structure commonly found in the atmospheric surface layer for time series of temperature, water vapour and other scalars (e.g. Barthlott et al. 2007). Note that for weak stable stratification, the flux may even be overestimated with the scalar sensor downwind of the sonic.

We noted previously that the difference in flux attenuation for the scalar sensor either upwind or downwind of the sonic is determined by the second term in the integrand of Eq. 9, the quadrature spectrum multiplied by $\sin(k_x r_x)$, which is an antisymmetric function of r_x. With the exception of weak unstable stratification, $-0.1 < z/L < 0$, the quadrature spectrum is opposite in sign to the cospectrum at high wavenumbers, roughly $k > k_{mx}$, causing the flux attenuation at small $k_{mx}|r_x|$ to be less for the scalar sensor downwind of the anemometer. Equivalently the time series of T_c leads w by about 5–10° for $|z/L| > 0.1$, but up to 15–25° as the amplitude of the cospectra decreases for near-neutral stratification. (At small wavenumbers, the sign of the quadrature spectrum commonly varies rapidly with wavenumber but in some cases can also have the same sign as the cospectrum over a finite band of wavenumbers.) Note from Eq. 9 that the attenuation calculated from just the cospectrum term is exactly midway between the attenuations calculated by including the quadrature spectrum term for positive and negative r_x. For each individual HATS case, we find that the flux attenuation calculated with Eq. 9 agrees very closely with that simulated by Eq. 14 for both positive and

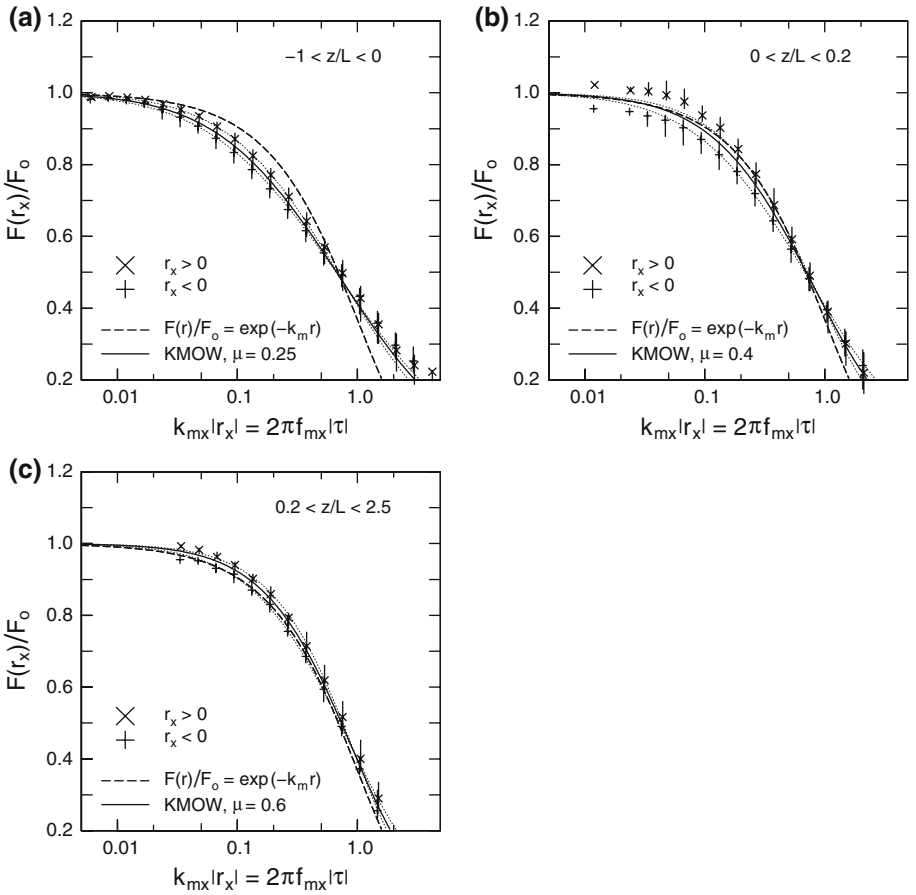

Fig. 5 **a** Flux attenuation for streamwise sensor displacements and unstable stratification. The fine-dotted lines are empirical fits for $r_x > 0$ and $r_x < 0$. **b** Flux attenuation for streamwise sensor displacements as for **a**, but for weak stable stratification, $0 < z/L < 0.2$. **c** Flux attenuation for streamwise sensor displacements as for **a**, but for strong stable stratification, $0.2 \leq z/L$

negative streamwise sensor displacements. This is not unexpected, because Eq. 14 written as an integral over the cross spectrum as a function of frequency has the same form as Eq. 6, from which Eq. 9 was derived.

As suggested by the empirical cospectral relations used in Fig. 3, $F(r_x)/F_o$ as a function of $k_{mx}r_x$ is noticeably different for stable and unstable stratification. It also has a smaller, but systematic, difference between weak and strong stable stratification. Curves are shown in Fig. 5a–c for both the exponential attenuation model, Eq. 13, and for numerical integration of the KMOW cospectrum, Eq. 10. The mean of the HATS data for positive and negative r_x is matched quite closely by Eq. 10 with $\mu = 0.25$ for unstable stratification, 0.4 for weak stable stratification ($0 < z/L \leq 0.2$), and 0.6 for strong stable stratification ($0.2 < z/L$). A notable exception is $F(r)/F_o < 0.5$ for unstable stratification, which depends on the highly variable low-wavenumber range of the unstable cospectrum. The stably stratified HATS data are also matched reasonably well by the exponential model, again with the exception of $F(r)/F_o < 0.5$. As will be shown, k_{mx} varies over a wide range for stable stratification, and

thus without k_{mx} in the abscissa, the data would not collapse as closely to a single relation as seen here.

The small values of the phase angle between w and T_c suggest that accurate estimates of the quadrature spectrum are difficult to obtain. As a consequence, the high variability of the quadrature spectra has not made it possible to fit them with universal curves as a function of z/L. Rather, fine-dotted curves are shown in Fig. 5 for separate empirical fits to the observations for positive and negative sensor displacements. These fits use numerical integrations of the KMOW cospectrum with values of μ chosen to provide an 'eyeball fit' to the composited observations. The values chosen for μ are 0.3 and 0.22 for unstable stratification with the scalar sensor, respectively, downwind and upwind of the sonic, 0.5 and 0.3 for weak stable stratification, and 0.75 and 0.45 for strong stable stratification. Note that for weak stable stratification, the KMOW cospectral model cannot match the values of $F(r_x)/F_o$ that depart significantly from unity at small $k_{mx}r_x$ and are a consequence of the quadrature spectrum's having a magnitude comparable to or exceeding the cospectrum at high wavenumbers.

Figure 6 shows $n_{mx} = f_m z/U$ as a function of z/L for the HATS data. For unstable stratification, n_{mx} is roughly constant, but exhibits a great deal of scatter, which is associated with large case-to-case variations in the low-wavenumber portion of the scalar flux cospectrum (Appendix A). However for near-neutral and stable stratification, n_{mx} increases systematically with z/L, changing by a factor greater than 10. This overall behaviour is identical to that found by Kaimal and Finnigan (1994) with previous datasets. The HATS data are approximated by the empirical relation,

$$n_{mx} = \begin{cases} 0.07, & z/L \le -0.1, \\ 2.31 - 2.24/(1.015 + 0.15z/L)^2, & z/L > -0.1. \end{cases} \tag{15}$$

Evaluation of $k_{mx}r_x$ for the HATS data in Fig. 5 requires estimating the speed U_a at which eddies are advected, the eddy advection speed being required to both transform the time delay in Eq. 14 to a streamwise displacement $r_x = U_a\tau$, as well as transform the observed

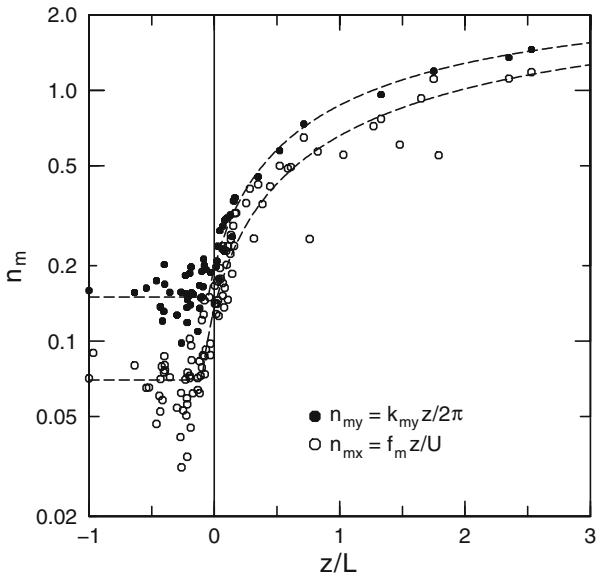

Fig. 6 Dimensionless frequency or wavenumber at the maxima of the streamwise and crosswind cospectra, as a function of z/L. Curves correspond to Eqs. 15 and 18

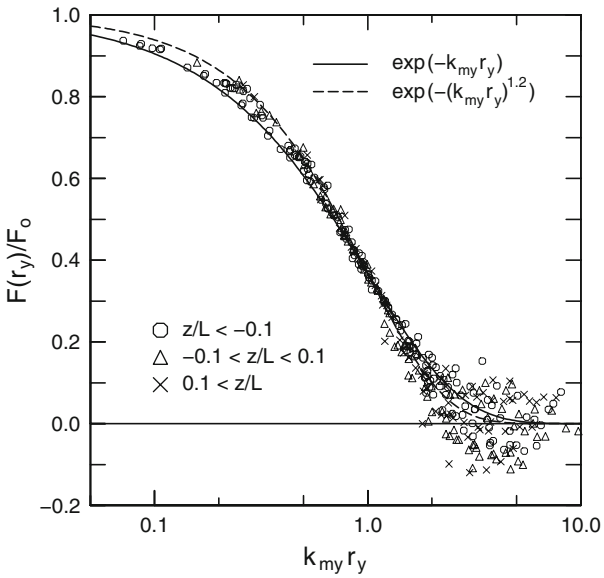

Fig. 7 Flux attenuation for crosswind sensor displacements

frequency of the cospectral maximum to a wavenumber, $k_{mx} = 2\pi f_m / U_a$. In Fig. 5 we have assumed that the same advection speed applies in both instances, and in that case the value of U_a is immaterial for evaluating $k_{mx} r_x$.

However, observations of atmospheric surface-layer turbulence suggest that U_a depends on eddy size, with small eddies advected at the local wind speed U while large eddies are advected at a speed greater than U (Appendix B). Thus, for simulating small sensor displacements $r_x = U\tau$, and for simulating large displacements $r_x = U_a \tau$ where $U_a/U > 1$. Unfortunately, neither the eddy size dividing these two regimes nor the advection speed of large eddies is well known. Estimation of the eddy advection speed from the HATS dataset is discussed in more detail in Appendix B. For application of the streamwise displacement model of Eqs. 10 and 15, r_x is known from the sensor configuration and it only remains to estimate k_{mx} from n_{mx}. The HATS data suggest that estimation of $k_{mx} = 2\pi f_{mx}/U_a = 2\pi n_{mx} U/zU_a$ requires $U_a/U \approx 1.1$.

4.2 Crosswind Sensor Displacements

The fluxes for crosswind sensor displacements, $F(r_y)$, were calculated after projecting the HATS data from each of the two arrays onto lines normal to the mean wind direction by lagging the data from each sonic by $\tau = jS \sin\theta_a / U$ (another use of Taylor's approximation). Here θ_a is the mean wind direction at each height relative to the array normal ($\theta_a = 0$ for wind normal to the array) and j is the integer position of each sonic in the array relative to the central sonic, e.g. for the nine-sonic d arrays, $-4 < j < 4$. Data for crosswind sensor displacements were limited to 29 cases with $F(r_y = S)/F_o > 0.25$ and, because of the need to project the data onto the crosswind direction, with wind directions within $\pm 33°$ of the array normal. The flux attenuation for each crosswind spatial displacement was determined by averaging together all sonic pairs with a given separation.

Application of Eq. 9 to crosswind sensor displacements requires an expression for the, generally unknown, dependence of the cospectrum on crosswind wavenumber. Instead, Fig. 7

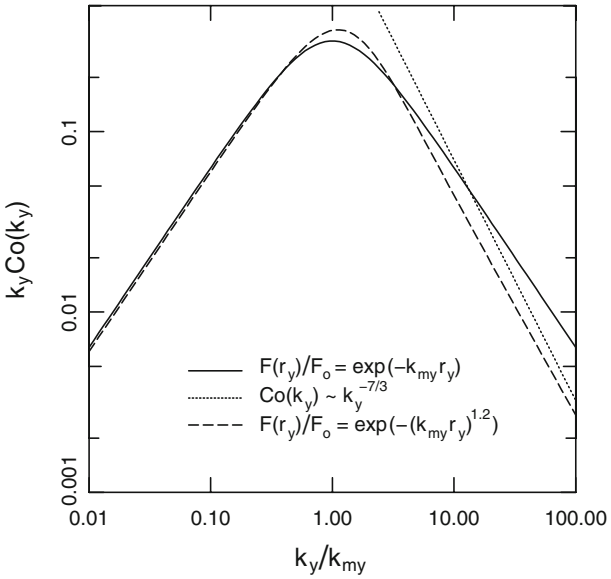

Fig. 8 Cospectra calculated with Eq. 17 for $b = 1$ and 1.2. Dotted line corresponds to $Co \sim k^{-7/3}$

shows the flux attenuation as a function of $k_{my}r_y$, where k_{my} was estimated for each data period and height by a fit of the exponential model, Eq. 13, to the crosswind flux attenuation data. As can be seen, the data correspond reasonably well to the exponential attenuation model, particularly for unstable stratification, but a better fit is found empirically to be

$$F(r_y) = F_o \exp\left(-(k_{my}r_y)^b\right). \tag{16}$$

The 'best fit' exponent b varies from 1.09 for unstable stratification, to 1.14 for neutral stratification, and 1.22 for stable stratification. The corresponding crosswind cospectrum is found from the cosine transform of $F(r_y)/F_o$,

$$Co(k_y) = \frac{2}{\pi}\int_0^\infty \exp\left(-(k_{my}r)^b\right)\cos(k_y r)\,\mathrm{d}r. \tag{17}$$

Figure 8 compares the crosswind cospectrum for Eq. 16 with $b = 1.2$ to that for the exponential model, Eq. 13. The high wavenumber cospectrum for $b > 1$ decreases at a rate faster than k^{-2} for the exponential model but still not as fast as the theoretical inertial range cospectrum, which is proportional to $k^{-7/3}$.

Figure 6 also shows $n_{my} = k_{my}z/2\pi$ as a function of z/L. The dependence of n_{my} on stability is very similar to that for n_{mx}, but n_{my} is systematically greater than n_{mx}, mainly because vertical shear elongates the eddies in the streamwise direction, placing the peak of the streamwise cospectrum at lower wavenumbers (e.g. Nicholls and Readings 1981). As a consequence, the scalar flux decays more slowly with sensor displacement in the streamwise direction than in the crosswind direction. For unstable stratification, the difference in decay rates is greater than a factor of 2, while for near-neutral stratification the difference is reduced to 44% and for strong stable stratification the difference is about 30%. The HATS data are approximated by the empirical relations,

$$n_{my} = \begin{cases} 0.15, & z/L \le -0.05, \\ 2.43 - 2.28/(1.01 + 0.2z/L)^2, & z/L > -0.05. \end{cases} \tag{18}$$

Note that in all but a few unstable cases, k_{my} obtained by a fit of the observations to Eq. 16 with $1.09 \le b \le 1.22$ differ by less than 5% from those estimated by a fit to the exponential model, $b = 1$.

4.3 Dependence on Wind Direction

We have separated the flux attenuation analysis into crosswind and streamwise sensor displacements, but the general case will be composed of some combination of the two displacements, $\mathbf{r} = (r_x, r_y)$. If the horizontal cross-section of an eddy is assumed to be elliptical, as suggested by Lee and Black (1994), then

$$\frac{1}{\lambda_m^2(\theta)} = \frac{\cos^2\theta}{\lambda_{mx}^2} + \frac{\sin^2\theta}{\lambda_{my}^2}, \tag{19}$$

or equivalently,

$$k_m(\theta) = (k_{mx}^2 \cos^2\theta + k_{my}^2 \sin^2\theta)^{1/2}, \tag{20}$$

where θ is again the wind direction relative to the sensor displacement (Fig. 1). LB's dependence on wind direction, Eq. 2, is similar to Eq. 20 and LB find that their data can be fitted with an implied value of $k_{my}/k_{mx} = \sqrt{2.4} = 1.55$. Correspondingly, Eqs. 15 and 18 for the HATS data give $1.46 \le k_{my}/k_{mx} \le 2.23$ for unstable to neutral stratification, the range of LB's data.

Then, since $\cos\theta = r_x/r$,

$$k_m r = (k_{mx}^2 r_x^2 + k_{my}^2 r_y^2)^{1/2}. \tag{21}$$

If it is further assumed that

$$A_x \equiv F(r_x)/F_o = \exp(-k_{mx} r_x), \tag{22}$$

$$A_y \equiv F(r_y)/F_o = \exp(-k_{my} r_y), \tag{23}$$

and

$$F(r_x, r_y)/F_o = \exp(-k_m r), \tag{24}$$

then

$$F(r_x, r_y) = F_o \exp\left[-\left(\ln^2 A_x + \ln^2 A_y\right)^{1/2}\right]. \tag{25}$$

Note that, with the exception of streamwise displacements combined with unstable stratification, Eqs. 22, 23 have been found to be good approximations to the HATS data.

The validity of Eq. 25 can be tested directly with the HATS data using observations of A_x, A_y, and $F(r_x, r_y)/F_o$. Figure 9 shows $F(r_x, r_y)/F_o$ for a moderately unstable case, $z/L = -0.4$, as a function of θ. The data are plotted separately for each of the eight crosswind sensor displacements available in the d array of the fourth HATS sonic configuration, with r_y/z ranging from 0.13 to 1.04. The discrete data points are the observed values of $F(r_x, r_y)/F_o$, with each point corresponding to a streamwise sensor displacement $nU\delta t$ where δt is the sample spacing of the time series data, viz. 0.05 s. The lines on the plot are the predictions of Eq. 25 using the corresponding observed values of A_x and A_y.

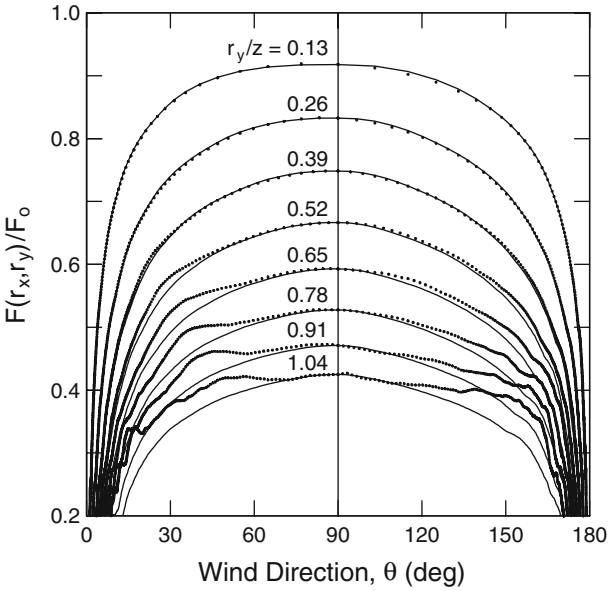

Fig. 9 Test of Eq. 25 for $F(r_x, r_y)/F_o$ as a function of wind direction relative to the sensor displacement; $r_x/z = 0.028n$, $z/L = -0.4$

As can be seen, Eq. 25 is identically valid for $\theta = 0°$, 90° and 180°. The errors increase with increasing sensor displacement, but for $F(r)/F_o \geq 0.6$, Eq. 25 is a very good approximation for all wind directions. The maximum errors occur for wind directions less than 45° and greater than 135° (or $r_x > r_y$) because the flux attenuation for a given sensor displacement is greater in the crosswind direction than in the streamwise direction. Similar results are found for all stabilities, although the errors in Eq. 25 are somewhat smaller for near-neutral and stable stratification, presumably because Eq. 22 is a better approximation for those conditions.

4.4 Model Tests

The comparison shown in Fig. 9 does not explicitly test the individual models for A_x and A_y. This is done in Fig. 10a where we again use Eq. 25 to combine streamwise and crosswind displacements, but estimate A_x and A_y with the simplest HATS model: Eqs. 10 and 15 for $F(r_x)$, using $\mu = 0.25$ for unstable, $\mu = 0.4$ for $0 < z/L < 0.2$, and $\mu = 0.6$ for $z/L \geq 0.2$, and Eqs. 13 and 18 for $F(r_y)$. The data points correspond to the median values of the model estimates within each interval of the measured values, and the vertical bars again denote the 15 and 85% quantiles of the estimated-flux-attenuation distribution within each interval. For $F(r)/F_o > 0.5$, the root-mean-squared deviation of the $F(r_x, r_y)/F_o$ estimates from the observations is on the order of 0.05, and a linear fit of the model estimates to the observations is $y = 1.01x - 0.01$.

A similar comparison of the Lee and Black (1994) model, Eqs. 1, 2, to the unstable HATS data in Fig. 10b shows that the model systematically overestimates $F(r_x, r_y)/F_o$ for values greater than 0.7 and underestimates for values less than 0.7. The underestimation of $F(r_x, r_y)/F_o$ for large attenuation increases with increasing flux attenuation, consistent with the analysis shown in Fig. 2.

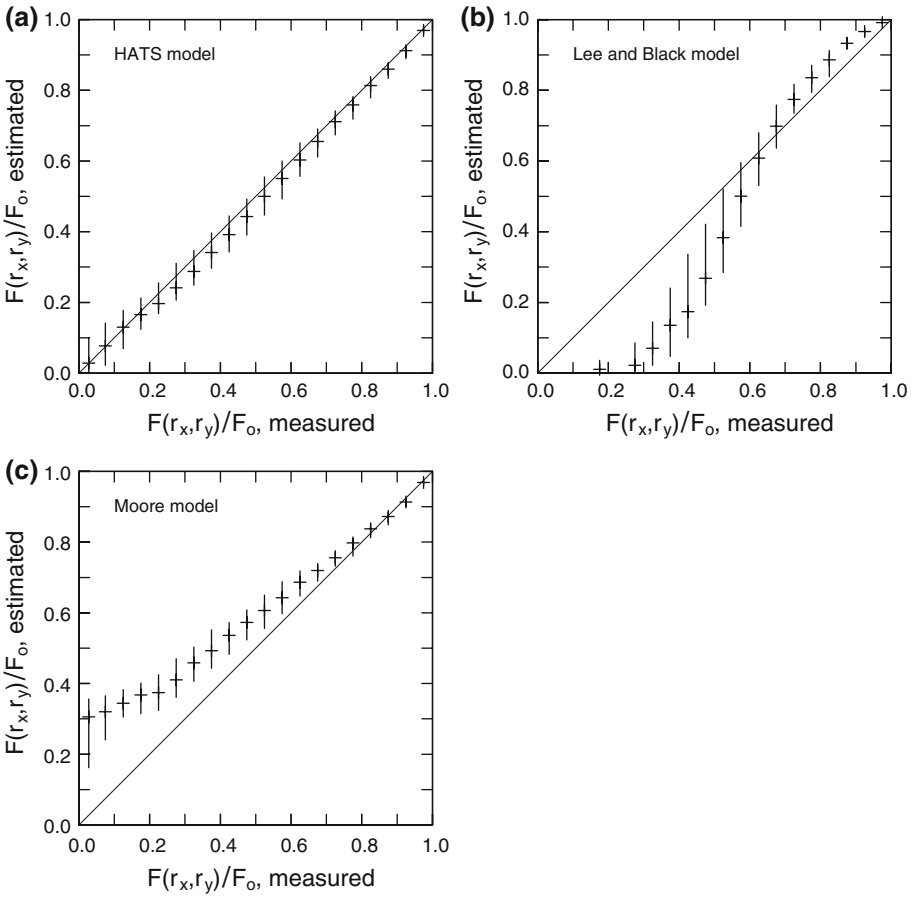

Fig. 10 **a** $F(r_x, r_y)/F_o$ for the HATS model vs. observations. **b** $F(r_x, r_y)/F_o$ for the LB94 model vs. observations. **c** $F(r_x, r_y)/F_o$ for the Moore (1986) model vs. observations

In Fig. 10c, we also compare the HATS measurements to the often-used flux attenuation model proposed by Moore (1986) for "sensors not widely separated". Moore assumes, like KMOW, that to a good approximation flux attenuation is independent of wind direction, and in the present notation,

$$F(r_x, r_y) = \int_{-\infty}^{\infty} Co_{wc}(k) \exp\left(-9.9(kr/2\pi)^{1.5}\right) \mathrm{d}k, \tag{26}$$

where again $r^2 \equiv r_x^2 + r_y^2$. Moore (1986) makes no distinction between streamwise and cross-wind cospectra, with the implied assumption that these are identical and equal to the Kansas streamwise cospectrum (Kaimal et al. 1972). Hence we evaluate Eq. 26 with the KMOW cospectral model, Eq. 4, using the values of μ and n_{mx} determined from HATS streamwise cospectra. For $F(r)/F_o > 0.85$, the estimates of the Moore model are in good agreement with the HATS data, consistent with the limitations placed on the model. For greater attenuation, the Moore model increasingly underestimates the observed flux attenuation.

5 Vertical Sensor Displacements

The HATS data can also be used to investigate scalar flux attenuation due to vertical displacement of the scalar sensor. KMOW again find little dependence of the flux attenuation on atmospheric stability and plot their data versus the height ratio z/z', where z is the height of the anemometer and z' is the height of the scalar sensor. Four unique values of z/z' are available from the HATS data, 2.09, 1.26, 0.79, and 0.48, while the measurement height, $z_{agl} - h_d$, ranges from 3.13 to 8.34 m (Table 1). Figure 11 shows $F(z, z')/F_o$ as a function of z/z', along with the KMOW relation for $F(z, z')/F_o = g(z/z')$, Eq. 5. The HATS data are in qualitative agreement with the KMOW relation and support the KMOW finding that flux attenuation is less for the scalar sensor located below the anemometer than for the opposite configuration.

The HATS data points are plotted separately for stable and unstable stratification, and it can be seen that the flux attenuation for stable stratification is generally greater than estimated by the KMOW relation and for unstable stratification is often less than estimated by KMOW. The height range of the KMOW data is 1–2.5 m and 90% of the KMOW data fall in the range $-0.1\ \mathrm{m}^{-1} < L^{-1} < 0.2\ \mathrm{m}^{-1}$ (Jakob Mann, personal communication, 2008), suggesting that Eq. 5 corresponds to near-neutral stratification.

Recall that KMOW were unable to provide a quantitative theoretical model for flux attenuation due to vertical sensor displacements, as is the case with us. Rather, we have tried two ad-hoc models to represent the dependence of flux attenuation on atmospheric stability: a linear model and an exponential model. The linear model is a generalization of the near-neutral KMOW model, Eq. 5,

$$F(z, z') = F_o[1 - D(z/z', z/L)\, r_z/z'], \tag{27}$$

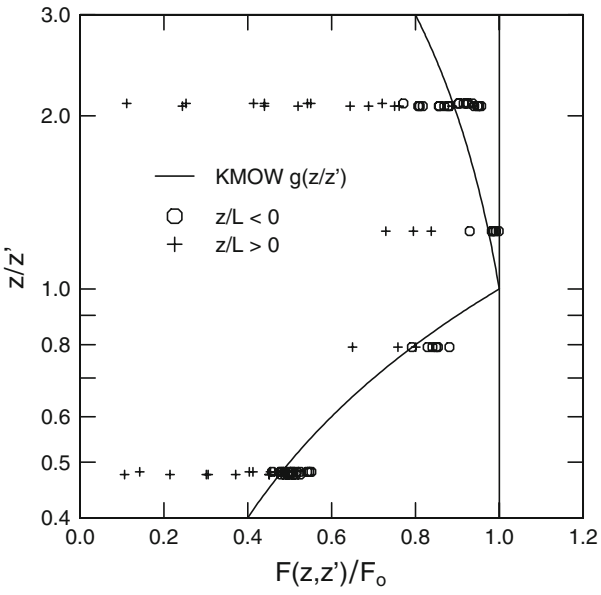

Fig. 11 Flux attenuation for vertical sensor displacement vs. z/z', where z is height of anemometer and z' is height of scalar sensor

where $r_z = |z - z'|$ and we assume that D depends on both z/z' and z/L. The exponential model corresponds to Eq. 13,

$$F(z, z') = F_o \exp(-k_{mz} r_z), \tag{28}$$

where we assume that k_{mz} also depends on both z/z' and z/L. (We have used the notation k_{mz} in Eq. 28 in order to facilitate comparison with corresponding variables for horizontal displacement, but we do not mean to imply that this parameter has the same physical meaning as the corresponding horizontal parameters.) These two models are similar for small values of Dr_z/z' or $k_{mz} r_z$, but the HATS data extend to sufficiently large values of r_z/z' to differentiate between the two models, particularly for $z/z' < 1$. The coefficients D and k_{mz} can be determined for each case of the HATS data from Eqs. 27 and 28 and plotted as a function of z/L and z/z'. We find that the collapse of the calculated coefficients to universal functions of stability, one for $z/z' < 1$ and another for $z/z' > 1$, is better with the exponential model than with the linear model.

Figure 12 shows $n_{mz} = k_{mz} z_{min}/2\pi$ for the HATS data as a function of z_{min}/L where z_{min} is the smaller of z and z'. (For both models we also tried, with less success, vertical length scales equal to z, z', z_{max} and $(z + z')/2$.) The observations in Fig. 12 are approximated with the empirical relations

$$n_{mz}(z/z' < 1) = \begin{cases} 0.1, & z_{min}/L \le 0.03, \\ 0.43 - 0.33/(0.964 + 1.2 z_{min}/L)^2, & z_{min}/L > 0.03, \end{cases} \tag{29}$$

and

$$n_{mz}(z/z' > 1) = \begin{cases} 0.013, & z_{min}/L \le -0.03, \\ 0.3 - 0.287/(1.051 + 1.7 z_{min}/L)^2, & z_{min}/L > -0.03. \end{cases} \tag{30}$$

Note that $k_{mz}(z/z' > 1)$ is less than $k_{mz}(z/z' < 1)$ for all observed stabilities, extending the observation of KMOW that $F(z/z' > 1) > F(z/z' < 1)$ to a broad range of stratification.

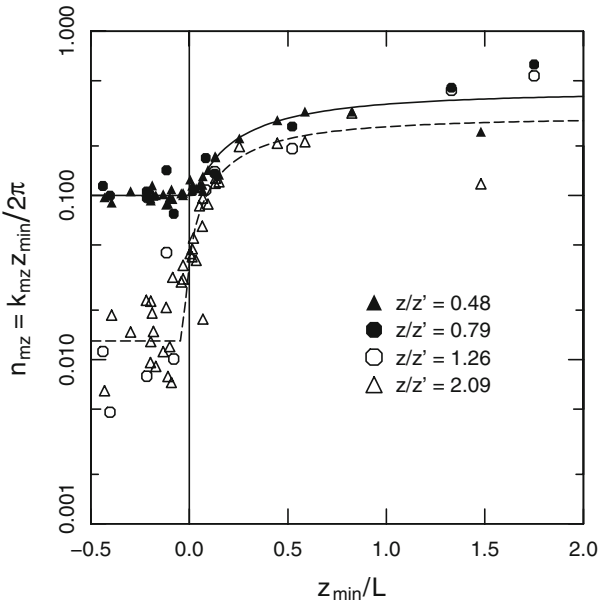

Fig. 12 n_{mz} for vertical sensor displacement vs. z_{min}/L

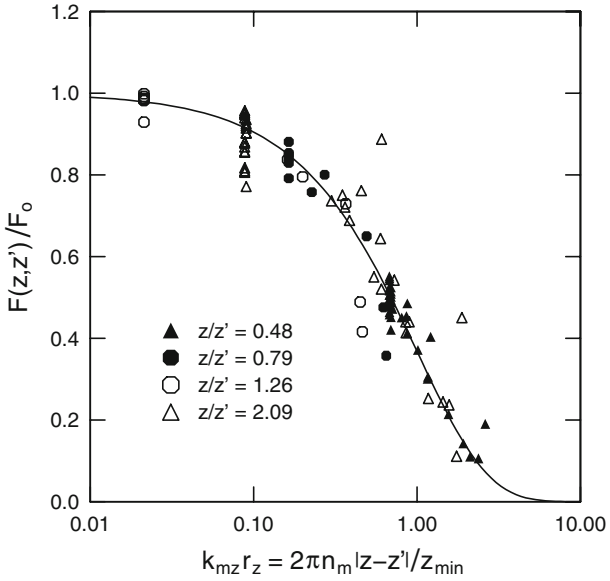

Fig. 13 Flux attenuation for vertical sensor displacement vs. $k_{mz}r_z$

Comparison of Fig. 12 with Fig. 6 similarly extends to a greater range of stratification the finding of KMOW that flux attenuation with the scalar sensor displaced below the anemometer is less than that for an equal horizontal displacement, particularly for unstable stratification.

Figure 13 compares $F(z, z')/F_o$ as a function of $k_{mz}r_z$ to the exponential model. Since the HATS data have only one pair of $F(z, z')/F_o$ and r_z for each case, the values of k_{mz} calculated from Eq. 28 identically satisfy the exponential model. Hence we have used the values of k_{mz} calculated from the empirical relations (29) and (30) to plot the points in Fig. 13. The vertically-aligned points correspond to unstable stratification, or constant values of k_{mz}, for each of the four unique vales of z/z', whereas the scattered points correspond to stable stratification where k_{mz} depends strongly on stability.

6 Conclusions and Discussion

The HATS data show that scalar flux attenuation for streamwise, crosswind, and vertical separations of the scalar and vertical velocity sensors are each a function of a dimensionless, stability-dependent parameter n_m multiplied by the ratio of sensor displacement to measurement height. Flux attenuation for horizontal displacements is a function of the magnitude and direction of the displacement and of the dependence of the $\overline{w'c'}$ cospectrum on stability and wavenumber. In the case of streamwise displacements, n_{mx} is the dimensionless wavenumber at the maximum of the wavenumber-weighted cospectrum. We find that flux attenuation for streamwise displacements can be estimated quite well by the integral of the KMOW cospectral relation, Eq. 10, using stability-dependent values for μ, a parameter describing the shape of the cospectrum, and for k_{mx}, the wavenumber at the peak of the cospectrum. However, there are small, systematic deviations of the HATS data from the KMOW model such that flux attenuation is often less for the scalar sensor downwind of the anemometer than

vice versa. These deviations are explained by the inclusion of the quadrature spectrum term in Eq. 9, which was neglected in the KMOW cospectral model.

Although the dependence of the $\overline{w'c'}$ cospectrum on the crosswind wavenumber is generally unknown, the attenuation due to crosswind sensor displacement can be estimated comparatively simply with the exponential model of Eq. 13. The HATS data show that the flux decays more rapidly for crosswind sensor displacements than for streamwise displacements and decays more rapidly for stable stratification than for unstable stratification. The assumption of the exponential model for both streamwise and crosswind attenuation permits a very simple expression, Eq. 25, for the dependence of flux attenuation on wind direction relative to the sensor displacement. That expression provides good estimates for $F(r)/F_o > 0.6$, even for unstable stratification where flux attenuation for streamwise displacements deviates from the exponential model.

Our estimates of flux attenuation for streamwise sensor displacements are based on the assumption of Taylor's frozen-field approximation. Thus if time series data are available, numerical integration of Eqs. 9 or 10 and specification of the cospectra and the (highly-variable) quadrature spectra can be avoided by using Taylor's approximation to simply lag the data from the scalar sensor by $\tau = -r_x/U_a$, the opposite sign from that used in Eq. 14. Since sensor displacements are commonly a small fraction of the measurement height, it is likely that $U_a \simeq U$, the local wind speed. Then from Eqs. 23 and 25, correction for attenuation due to any additional crosswind displacement is simply

$$F(0, r_y) = F(r_y) = F_o \exp(-k_{my} r_y). \tag{31}$$

Note that the common practice of choosing τ to maximize the correlation between w' and c' will not be strictly correct for streamwise displacements, because the phase angle between the two variables is generally non-zero. However, by comparing the observations in Fig. 5a–c to the solid lines for the KMOW model, it can be seen that the flux error caused by neglecting the antisymmetric part of Eq. 9 is on the order of 5% or less.

The HATS data extend to a broad range of stratification the observation of Kristensen et al. (1997) that flux attenuation is less for the scalar sensor located below the anemometer than for either an equal horizontal displacement or for the scalar sensor located an equal distance above the anemometer. As observed for horizontal displacements, we find that the flux measured with vertically-displaced sensors decreases more rapidly with increasing displacement for stable stratification than for unstable. Neither KMOW nor we have been able to derive a theoretical expression for flux attenuation caused by vertical sensor displacement and, consequently, we are limited to ad-hoc empirical relations to describe our observations. The HATS data suggest that the linear KMOW relation for $g(z/z')$, Eq. 5, applies best to near-neutral stratification. For a broader range of stratification, we find that an exponential model, Eqs. 28–30, is better able to collapse the observations into one universal relationship for $z/z' > 1$ and another for $z/z' < 1$. Matching the HATS model to the KMOW relation suggests that the latter applies for $z_{min}/L \approx -0.025$.

The HATS flux-attenuation observations were obtained with turbulence data measured within a horizontally-homogeneous, terrestrial surface layer, that is, where the turbulence structure is found to depend only on the height above the surface and on the surface fluxes of momentum and buoyancy as described by Monin-Obukhov similarity. The HATS flux attenuation relations are not valid where the dependence on wavenumber of the scalar-flux cospectrum differs materially from that in the terrestrial surface layer, as may be true for measurements in advective conditions, in complex terrain, over a wavy water surface, within a canopy, or within the roughness sublayer above the canopy. In these more complex situations, empirical, in-situ techniques such as suggested by Villalobos (1997) and Laubach and

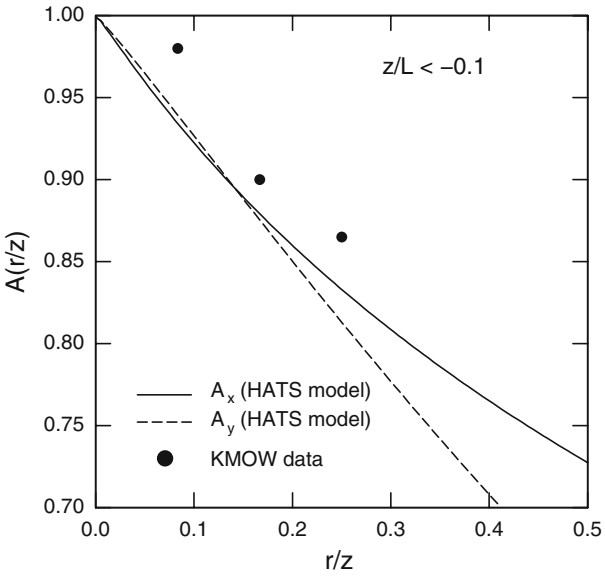

Fig. 14 Comparison of HATS models for A_x and A_y to KMOW data

McNaughton (1998) may be advantageous. These techniques utilize a temperature sensor placed near the scalar sensor to measure a displaced-sensor heat flux, which is then divided by the (co-located) sonic heat flux to determine the flux attenuation in real time. Drawbacks of this technique include the required assumption of scalar similarity, the vanishing heat flux for neutral stratification, and the necessity to correct the sonic virtual heat flux for the water vapour flux, e.g. Schotanus et al. (1983).

Finally, we return to two questions raised at the beginning of this paper. First, neither theoretical analysis nor comparison with the HATS data supports the dependence of flux attenuation on $(r/z)^{4/3}$ for other than very small values of the ratio r/z. However, except for a difference in the exponent, the HATS data do support a model of wind direction dependence similar to that of Lee and Black (1994), Eq. 2.

Second, the reason that Kristensen et al. (1997) find no dependence of flux attenuation on wind direction appears to be the limited range of their data, i.e. unstable stratification and $r/z \leq 0.25$. Within this range, the HATS flux attenuation model finds that $A_x = F(r_x)/F_o$ and $A_y = F(r_y{=}r_x)/F_o$ are within 4% or less of each other (Fig. 14). While $k_{my}{=}2.3\,k_{mx}$ for unstable stratification (Fig. 6), this difference is almost exactly compensated by the fact that, for the range of the KMOW data, A_x decreases more rapidly as a function of $k_{mx}r_x$ than does A_y as a function of $k_{my}r_y$. See Fig. 5a, where the exponential curve (with $k_{my}r_y = k_{mx}r_x$) represents the attenuation for crosswind displacements relative to the KMOW model for streamwise displacements.

Acknowledgements The authors are grateful to Leif Kristensen, Jakob Mann, David Gurarie, Gaby Katul, and Fabienne Lohou for helpful discussions. The National Center for Atmospheric Research is funded by the National Science Foundation.

Appendix A: Fit of the KMOW Cospectral Relation to HATS Data

In order to apply Eq. 10 to estimate flux attenuation caused by streamwise sensor displacements, we fit the KMOW cospectral relation, Eq. 4, to the HATS $\overline{w'T_c'}$ cospectra. The best fit was determined by minimizing the mean absolute error between the measured cospectrum and the KMOW relation, as a function of the two parameters μ and k_m or equivalently $n_m = f_m z/U$. Here, μ is a parameter that determines the shape of the cospectrum: larger values of μ correspond to broader cospectra. Figure 15 shows that μ is a systematic function of z/L, which can be approximated as

$$\mu = \begin{cases} 0.25, & z/L \le 0, \\ 0.25 + 1.75 z/L, & 0 \le z/L \le 0.2, \\ 0.6, & z/L > 0.2. \end{cases} \tag{32}$$

Since it was seen from Fig. 6 that n_m is also a systematic function of z/L, it is expected that n_m and μ are closely related. This is shown in Fig. 16, where we note in particular that n_m and μ appear to also be correlated for unstable stratification, $\mu < 0.3$, implying that the scatter in n_m within that region is not merely variation of the cospectral maximum but is also directly related to changes in the cospectral shape. The data are closely fit with $n_m = 1.47\mu^{2.1}$.

The turbulence resolved by a sonic anemometer is attenuated at high wavenumbers by sonic path averaging (Kaimal et al. 1968; Horst and Oncley 2006). If the $\overline{w'T_c'}$ covariance measured during HATS is attenuated significantly by sonic path averaging, this will systematically reduce the empirical estimates of flux attenuation caused by sensor displacement. Including sonic path averaging,

$$F(r, p) = \int_{-\infty}^{\infty} Co_{wc}(k_1) \cos(k_1 r) H(k_1 p)\, \mathrm{d}k_1, \tag{33}$$

where we simplify Eq. 9 by ignoring the quadrature spectrum term and also assume that the displacement (and thus k_1) is in the streamwise direction; p is the sonic path length, 0.115 m

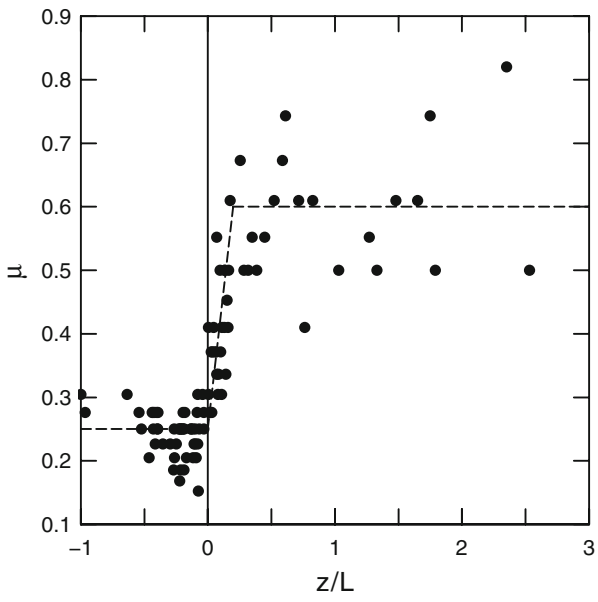

Fig. 15 μ as a function of z/L

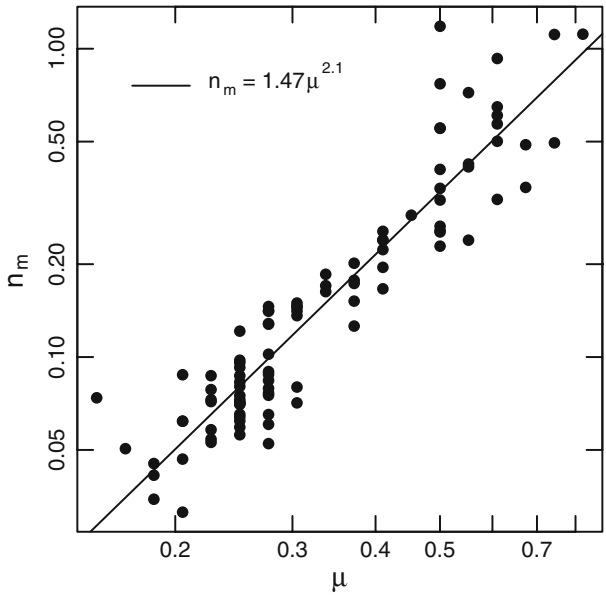

Fig. 16 n_m as a function of μ

in the case of the CSAT3 used in HATS. $H(k_1 p)$ is the transfer function for attenuation of scalar fluxes by path averaging, for which we use the calculations of Van Dijk (2002) for a CSAT3 combined with a sensor measuring scalar concentrations at the intersection of the sonic measurement paths. We have calculated HATS flux attenuation both with and without sonic path averaging using the KMOW cospectral model with μ varying between 0.2 and 0.8, corresponding to a wide range of z/L. The differences in flux attenuation increase with μ and z/L, but in all cases are on the order of 1% or less. Note that Van Dijk's H is for a point measurement of scalar concentration, whereas the HATS data use a path-averaged value of virtual temperature. Unfortunately, H has not been calculated for sonic measurements of the virtual temperature flux, but it would most likely be smaller than that calculated by Van Dijk (2002).

Appendix B: Determination of the Turbulence Advection Velocity

Investigations of Taylor's frozen-field approximation in the atmospheric surface layer by Panofsky et al. (1974) and Mizuno and Panofsky (1975) found that the eddy advection speed U_a depends on eddy size, with small eddies advected at the local wind speed U while large eddies are advected at a speed greater than U. However, they did not specify either the eddy size dividing these two regimes or the advection speed of large eddies. With the general support of wind-tunnel measurements, theoretical studies of inertial and dissipation range turbulence assume that small eddies are advected at the local wind speed (e.g. Antonia et al. 1980). Measurements by Favre et al. (1964, 1967) in a wind-tunnel turbulent boundary layer of depth δ found that near the wall, i.e. $z/\delta \leq 0.23$, U_a/U decreases with increasing frequency, from a maximum value greater than 1 at the lowest frequency of 8.7 Hz to values near 1 for frequencies above 100 Hz. Values of U_a/U were also found to decrease with distance

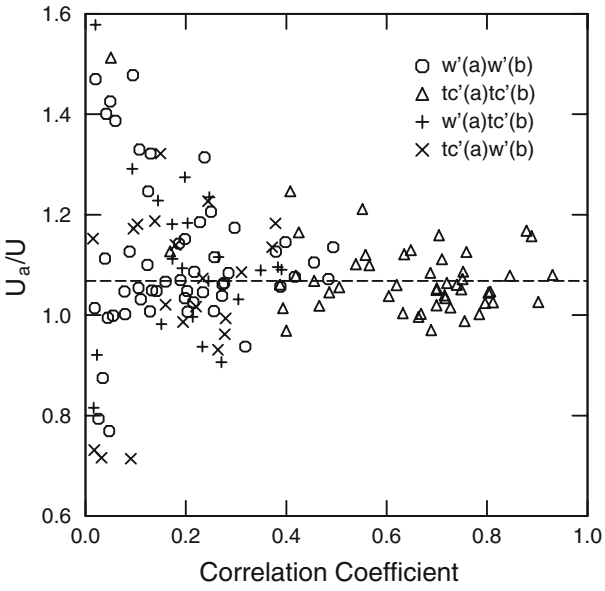

Fig. 17 The velocity ratio U_a/U as a function of the correlation coefficient between pairs of variables for lag t_m

from the wall, from 1.12–1.15 at $z/\delta = 0.03$ to values near 1 for $z/\delta > 0.23$. Measurements at a height of 15 m in the atmospheric surface layer by Powell and Elderkin (1974) found U_a/U in the range of 1.1–1.2. Although Powell and Elderkin calculated phase spectra from their data, they do not comment on the possibility of a dependence of U_a on eddy size. (We do not consider here the consequences of a fluctuating, i.e. turbulent, advection velocity.)

In order to directly measure the eddy advection speed during HATS, two additional towers were erected that were displaced parallel to the prevailing wind direction and thus normal to the horizontal sonic arrays. These towers, labeled a and b, were located approximately 80 m laterally from the horizontal sonic arrays, with tower a nominally downwind of tower b. Two sonics were placed on each of the two towers at the same heights as the two horizontal sonic arrays. The separation of these two towers, x_{ab}, was 26.8 m for the first configuration and 17.3 m for the other three. Except for the fourth configuration, this corresponds to the span of the nine-sonic d array. The corresponding separation for the fourth configuration would have placed tower b about 3 m upwind of the sonic on tower a, which would have distorted the flow at the downwind sonic.

The eddy advection speed was estimated as $x_{ab} \cos\beta / t_m$, where β is the wind direction relative to the line connecting the two towers and t_m is the time lag found to produce maximum correlation between turbulence variables measured at the two towers. Maximum correlation coefficients and eddy advection speeds were calculated for vertical velocity w measured at the two towers, for sonic temperature T_c measured at the two towers, and for w measured at one tower and T_c measured at the other. Figure 17 shows the velocity ratio U_a/U plotted as a function of the correlation coefficient between the two variables for lag t_m. The data in Fig. 17 are limited to $|\beta| < 15°$, since Horst et al. (2004) noted that the peak correlation coefficient decreases when $|\beta|$ exceeds that limit. For peak correlation coefficients greater than 0.3, the median value of U_a/U is 1.07. Note that most of the U_a/U data with peak correlation coefficients greater than 0.3 come from correlations between sonic temperature measured at both towers. There is no discernible trend of U_a/U with correlation coefficient, height or wind speed (not shown), but in Fig. 18 we see that there is a noticeable trend with

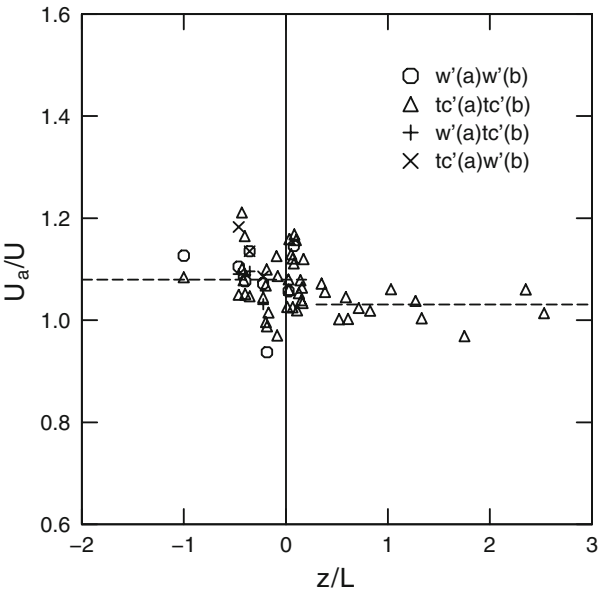

Fig. 18 $U_a/U = x_{ab}\cos\beta/Ut_m$ as a function of z/L, for correlation coefficients greater than 0.3

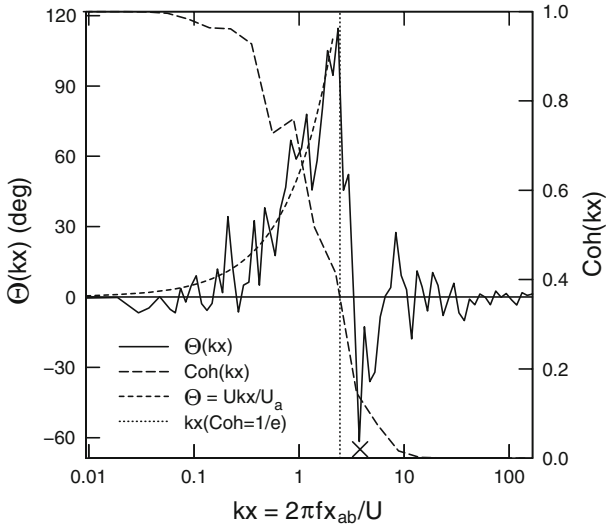

Fig. 19 Phase and coherence spectra, $z/L = 0.01$. X $= k_{mx}x_{ab}$

z/L. For $z/L < 0.2$, the median value of U_a/U is 1.08 and, for $z/L > 0.2$, the median value is 1.03.

In order to examine the dependence of the advection speed on eddy size or wavenumber, the phase spectra $\Theta(f)$ for T_c measured at the two towers were fit with

$$\Theta(f) = b2\pi f x_{ab}/U. \tag{34}$$

The slope of the linear fit, b, was determined by minimizing the absolute value of the deviations from Eq. 34 over the frequency range $0 < f \leq f_{e^{-1}}$, where $f_{e^{-1}}$ is the frequency

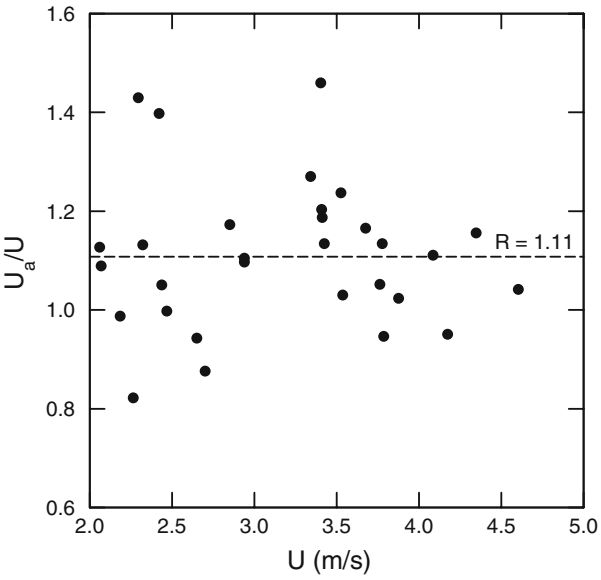

Fig. 20 U_a/U from linear fits to the phase spectra, as a function of wind speed

at which the coherence spectrum $Coh(f)$ is equal to e^{-1} (Powell and Elderkin 1974). The slope b is then equated to U/U_a.

Figure 19 shows an example of the phase and coherence spectra for a near-neutral HATS case, $z/L = 0.01$, plotted as a function of the wavenumber $k = 2\pi f/U$ normalized by x_{ab}. The coherence generally drops to e^{-1} for values of kx_{ab} between 1 and 3, as is also the case here. For $k < k_{e^{-1}}$ the phase spectrum follows Eq. 34, but as the coherence decreases to zero for larger values of k, the phase spectrum becomes ill-defined with a mean value near zero. Figure 20 shows the values of U_a/U derived from linear fits to the phase spectra and plotted as a function of wind speed, again for HATS cases with $|\beta| < 15°$. There is no significant dependence of U_a/U derived from the phase spectra on z/L (not shown), but the scatter decreases for wind speeds above $3.5\,\mathrm{m\,s^{-1}}$ and the median value of U_a/U in that range of wind speeds is 1.05. The overall median value of U_a/U is 1.11, and inspection of the phase spectrum plots for each of the cases in Fig. 20 suggests no dependence of U_a/U on wavenumber for $k < k_{e^{-1}}$. The X on the abscissa of Fig. 19 is the value of $k_{mx}x_{ab}$ for that case. For unstable and near-neutral stratification k_{mx} is on the order of $k_{e^{-1}}$, suggesting that $U_a(k_{mx})/U \approx 1.1$. For strong stability, $k_{mx} \gg k_{e^{-1}}$ and we can only speculate that there also $U_a(k_{mx})/U$ equals its value at lower wavenumbers.

References

Antonia RA, Phan-Thien N, Chambers AJ (1980) Taylor's hypothesis and the probability density functions of temporal velocity and temperature derivatives in a turbulent flow. J Fluid Mech 100:193–208

Barthlott C, Drobinski P, Fesquet C, Dubos T, Pietras C (2007) Long-term study of coherent structures in the atmospheric surface layer. Boundary-Layer Meteorol 125:1–24

Favre A, Gaviglio J, Fohr JP (1964) Répartition spectrale de corrélations spatio-temporelles de vitesse, en couche limite turbulente. In: Görtler H (ed) Proceedings of the 11th international congress of applied mechanics, Munich, 1964. Springer-Verlag, Berlin, 1966, pp 878–888

Favre A, Gaviglio J, Dumas R (1967) Structure of velocity space-time correlations in a boundary layer. Phys Fluids 10(Part II):S138–S145

Hill R (1989) Implications of Monin–Obukhov similarity theory for scalar quantities. J Atmos Sci 46: 2236–2244
Horst TW (1997) A simple formula for attenuation of eddy fluxes measured with first-order-response scalar sensors. Boundary-Layer Meteorol 82:219–233
Horst TW, Oncley SP (2006) Corrections to inertial-range power spectra measured by CSAT3 and Solent sonic anemometers. Boundary-Layer Meteorol 119:375–395
Horst TW, Kleissl J, Lenschow DH, Meneveau C, Moeng C-H, Parlange MB, Sullivan PP, Weil JC (2004) HATS: field observations to obtain spatially filtered turbulence fields from crosswind arrays of sonic anemometers in the atmospheric surface layer. J Atmos Sci 61:1566–1581
Kaimal JC, Finnigan JJ (1994) Atmospheric boundary layer flows. Oxford University Press, UK, 289 pp
Kaimal JC, Wyngaard JC, Haugen DA (1968) Deriving power spectra from a three-component sonic anemometer. J Appl Meteorol 7:827–837
Kaimal JC, Wyngaard JC, Izumi Y, Cote OR (1972) Spectral characteristics of surface-layer turbulence. Q J R Meteorol Soc 98:563–589
Kristensen L, Mann J, Oncley SP, Wyngaard JC (1997). How close is close enough when measuring scalar fluxes with displaced sensors? J Atmos Ocean Technol 14:814–821
Laubach J, McNaughton KG (1998) A spectrum-independent procedure for correcting eddy fluxes measured with separated sensors. Boundary-Layer Meteorol 89:445–467
Lee X, Black TA (1994) Relating eddy correlation sensible heat flux to horizontal sensor separation in the unstable atmospheric surface layer. J Geophys Res 99(D9):18545–18553
Lumley JL, Panofsky HA (1964) The structure of atmospheric turbulence. Wiley, New York, 239 pp
Mizuno T, Panofsky HA (1975) The validity of Taylor's hypothesis in the atmospheric surface layer. Boundary-Layer Meteorol 9:375–380
Moore CJ (1986) Frequency response corrections for eddy correlation systems. Boundary-Layer Meteorol 37:17–35
Nicholls S, Readings CJ (1981) Spectral characteristic of surface layer turbulence over the sea. Q J R Meteorol Soc 107:591–614
Panofsky HA, Thompson DW, Sullivan DA, Moravek DE (1974) Two-point velocity statistics over Lake Ontario. Boundary-Layer Meteorol 7:309–321
Powell DC, and Elderkin CE (1974) An investigation of the application of Taylor's hypothesis to atmospheric boundary layer turbulence. J Atmos Sci 31:990–1002
Schotanus P, Nieuwstadt FTM, DeBruin HAR (1983) Temperature measurement with a sonic anemometer and its application to heat and moisture fluctuations. Boundary-Layer Meteorol 26:81–93
Taylor GI (1938) The spectrum of turbulence. Proc Roy Soc London A165:476–484
Van Dijk A (2002) Extension to 3D of "The effect of line averaging on scalar fluxes measured with a sonic anemometer near the surface" by Kristensen and Fitzjarrald. J Atmos Ocean Technol 19:80–82
Villalobos FJ (1997) Correction of eddy covariance water vapour flux using additional measurements of temperature. Agric For Meteorol 88:77–83
Wyngaard JC (1988) Flow-distortion effects on scalar flux measurements in the surface layer: implications for sensor design. Boundary-Layer Meteorol 42:19–26